



HAL
open science

Identification, validation and biological characterisation of novel glioblastoma tumour microenvironment subtypes: implications for precision immunotherapy

K. White, K. Connor, M. Meylan, A. Bougoüin, M. Salvucci, F. Bielle, A.C.
O'farrell, K. Sweeney, L. Weng, G. Bergers, et al.

► To cite this version:

K. White, K. Connor, M. Meylan, A. Bougoüin, M. Salvucci, et al.. Identification, validation and biological characterisation of novel glioblastoma tumour microenvironment subtypes: implications for precision immunotherapy. *Annals of Oncology*, 2022, 34 (3), pp.300-314. 10.1016/j.annonc.2022.11.008 . hal-04090913

HAL Id: hal-04090913

<https://u-paris.hal.science/hal-04090913>

Submitted on 13 Apr 2024

HAL is a multi-disciplinary open access archive for the deposit and dissemination of scientific research documents, whether they are published or not. The documents may come from teaching and research institutions in France or abroad, or from public or private research centers.

L'archive ouverte pluridisciplinaire **HAL**, est destinée au dépôt et à la diffusion de documents scientifiques de niveau recherche, publiés ou non, émanant des établissements d'enseignement et de recherche français ou étrangers, des laboratoires publics ou privés.



Distributed under a Creative Commons Attribution - NonCommercial - NoDerivatives 4.0
International License

ORIGINAL ARTICLE

Identification, validation and biological characterisation of novel glioblastoma tumour microenvironment subtypes: implications for precision immunotherapy

K. White^{1†‡}, K. Connor^{1†‡}, M. Meylan², A. Bougouïn², M. Salvucci^{1†}, F. Bielle^{3†}, A. C. O'Farrell^{1†}, K. Sweeney⁴, L. Weng^{5†}, G. Bergers^{5†}, P. Dicker⁶, D. M. Ashley⁷, E. S. Lipp⁷, J. T. Low⁷, J. Zhao⁸, P. Wen⁹, R. Prins¹⁰, M. Verreault^{3†}, A. Idbaih^{11†}, A. Biswas^{1†}, J. H. M. Prehn^{1†}, D. Lambrechts^{12,13†}, I. Arijs^{12,13†}, F. Lodi^{12,13†}, G. Dilcan^{12,13†}, M. Lamfers^{14†}, S. Leenstra^{14†}, F. Fabro^{14†}, I. Ntafoulis^{14†}, J. M. Kros¹⁵, J. Cryan¹⁶, F. Brett¹⁶, E. Quissac³, A. Beausang¹⁶, S. MacNally⁴, P. O'Halloran⁴, J. Clerkin⁴, O. Bacon¹⁶, A. Kremer^{17†}, R. T. Chi Yen^{17†}, F. S. Varn¹⁸, R. G. W. Verhaak^{18,19}, C. Sautès-Fridman^{2†}, W. H. Fridman^{2†} & A. T. Byrne^{1*†}

¹Department of Physiology and Medical Physics, Royal College of Surgeons in Ireland, Dublin, Ireland; ²Centre de Recherche des Cordeliers, INSERM, Sorbonne Université, USPC, Université de Paris, Paris; ³Paris Brain Institute (ICM), CNRS UMR 7225, Inserm U 1127, UPMC-P6 UMR S 1127, Hôpital de la Pitié—Salpêtrière, Paris, France; ⁴National Centre of Neurosurgery, Beaumont Hospital, Dublin, Ireland; ⁵VIB-KU Leuven Center for Cancer Biology, Department of Oncology, Leuven, Belgium; ⁶Epidemiology & Public Health, Royal College of Surgeons in Ireland, Dublin, Ireland; ⁷Duke Cancer Institute, Duke University, Durham; ⁸Department of Systems Biology at Columbia University, New York; ⁹Center for Neuro-Oncology, Dana-Farber Cancer Institute, Boston; ¹⁰Department of Medical and Molecular Pharmacology, David Geffen School of Medicine, University of California, Los Angeles, USA; ¹¹Sorbonne Université, Inserm, CNRS, UMR S 1127, Paris Brain Institute (ICM), AP-HP, Hôpitaux Universitaires La Pitié Salpêtrière—Charles Foix, Paris, France; ¹²Laboratory for Translational Genetics, Department of Human Genetics, Leuven; ¹³VIB Center for Cancer Biology, Leuven, Belgium; ¹⁴Department of Neurosurgery, Brain Tumor Center, Erasmus University Medical Center, Rotterdam; ¹⁵Department of Pathology, Erasmus Medical Center, Rotterdam, The Netherlands; ¹⁶Department of Neuropathology, Beaumont Hospital, Dublin, Ireland; ¹⁷Information Technology for Translational Medicine (ITTM), Luxembourg, Luxembourg; ¹⁸The Jackson Laboratory for Genomic Medicine, Farmington, USA; ¹⁹Department of Neurosurgery, Cancer Center Amsterdam, Amsterdam University Medical Centers, VU University Medical Center, Amsterdam, The Netherlands



Available online 6 December 2022

Background: New precision medicine therapies are urgently required for glioblastoma (GBM). However, to date, efforts to subtype patients based on molecular profiles have failed to direct treatment strategies. We hypothesised that interrogation of the GBM tumour microenvironment (TME) and identification of novel TME-specific subtypes could inform new precision immunotherapy treatment strategies.

Materials and methods: A refined and validated microenvironment cell population (MCP) counter method was applied to >800 GBM patient tumours (GBM-MCP-counter). Specifically, partition around medoids (PAM) clustering of GBM-MCP-counter scores in the GLIOTRAIN discovery cohort identified three novel patient clusters, uniquely characterised by TME composition, functional orientation markers and immune checkpoint proteins. Validation was carried out in three independent GBM-RNA-seq datasets. Neoantigen, mutational and gene ontology analysis identified mutations and uniquely altered pathways across subtypes. The longitudinal Glioma Longitudinal AnalySiS (GLASS) cohort and three immunotherapy clinical trial cohorts [treatment with neoadjuvant/adjuvant anti-programmed cell death protein 1 (PD-1) or PSVRIPO] were further interrogated to assess subtype alterations between primary and recurrent tumours and to assess the utility of TME classifiers as immunotherapy biomarkers.

Results: TME^{High} tumours (30%) displayed elevated lymphocyte, myeloid cell immune checkpoint, programmed cell death protein 1 (PD-1) and cytotoxic T-lymphocyte-associated protein 4 transcripts. TME^{High}/mesenchymal+ patients featured tertiary lymphoid structures. TME^{Med} (46%) tumours were enriched for endothelial cell gene expression profiles and displayed heterogeneous immune populations. TME^{Low} (24%) tumours were manifest as an 'immune-desert' group. TME subtype transitions upon recurrence were identified in the longitudinal GLASS cohort. Assessment of GBM immunotherapy trial datasets revealed that TME^{High} patients receiving neoadjuvant anti-PD-1

*Correspondence to: Prof. Annette T. Byrne, Department of Physiology and Medical Physics, Royal College of Surgeons in Ireland, 123 St Stephens Green, Dublin 2, Ireland. Tel: +353-01-402-8673

E-mail: annettebyrne@rcsi.ie (A. T. Byrne).

[†]Member of the GLIOTRAIN consortium (<https://www.gliotrain.eu/>).

[‡]These authors contributed equally.

0923-7534/© 2022 The Authors. Published by Elsevier Ltd on behalf of European Society for Medical Oncology. This is an open access article under the CC BY-NC-ND license (<http://creativecommons.org/licenses/by-nc-nd/4.0/>).

had significantly increased overall survival ($P = 0.04$). Moreover, TME^{High} patients treated with adjuvant anti-PD-1 or oncolytic virus (PVSRIPO) showed a trend towards improved survival.

Conclusions: We have established a novel TME-based classification system for application in intracranial malignancies. TME subtypes represent canonical '*termini a quo*' (starting points) to support an improved precision immunotherapy treatment approach.

Key words: IDHwt glioblastoma, tumour microenvironment, subtypes, immunotherapy, precision therapy

INTRODUCTION

Elucidation of isocitrate dehydrogenase wild-type (IDHwt) glioblastoma (GBM) (referred to throughout as 'GBM' based on recent c-IMPACT-NOW¹ recommendations) disease subtypes¹ based on mutational profiling, gene expression and DNA methylation has failed to translate into improved clinical outcomes.² GBM tumours are complex ecosystems composed of diverse malignant (e.g. stem) and non-malignant (e.g. glial, microglia, immune cells, vascular cells, reactive astrocytes) cell populations which exist in several niches, interact with heterogeneous tumour cells³ and exhibit a dynamic heterogeneity and plasticity. Of late, there has been much focus on targeting the GBM immune cell niche, notwithstanding a generalised immunosuppressive microenvironment in the intracranial setting. For example, as the immune checkpoint protein programmed death-ligand 1 (PD-L1) is expressed in GBM^{4,5} and pre-clinical data^{6,7} provided rationale for evaluation of immune checkpoint inhibitors (ICIs), multiple clinical studies have now been completed. Disappointingly, these trials have been negative⁸⁻¹² most likely, as limited patient stratification methods were available to rationally select patients who might benefit most from treatment. Nevertheless, a small multicentre randomised controlled trial conducted in the setting of recurrent GBM (rGBM) suggests that neoadjuvant anti-programmed cell death protein 1 (PD-1) blockade may elicit enhanced immune responses and survival benefits.¹³

In the current study, the GLIOTRAIN consortium (www.gliotrain.eu), together with US collaborators, have interrogated tissue-infiltrating immune and stromal cell populations of selected GBM patients using a modified targeted microenvironment cell population counter (MCP-counter) RNA-seq computational method.¹⁴ Unsupervised partition around medoids (PAM) clustering identified three novel TME-associated subtypes designated TME^{Low}, TME^{Med} and TME^{High} which have been validated in publicly available datasets. To provide insight into novel subtype-specific biology, we analysed TME functional orientation markers and differentially expressed genes. Moreover, we carried out mutational analysis and neoantigen prediction across novel subtypes and have longitudinally assessed subtype switching events in primary and recurrent tumours. Finally, the capacity of novel TME subtypes to predict outcome was assessed in retrospective immunotherapy clinical trial datasets. Our findings lay the foundation for a novel subtyping approach which may be applied, to direct novel combinatorial immunotherapy strategies in the brain tumour setting.

MATERIALS AND METHODS

Patient series (n = 867 samples, N = 8 cohorts)

GLIOTRAIN discovery cohort. Informed consent for use of multi-omics data and associated clinical annotation was obtained via appropriate institutional channels. The GLIOTRAIN cohort comprised 123 retrospectively collected fresh frozen (FF) GBM samples, acquired at the time of surgery, with corresponding clinical follow-up data. Patient samples were collected based on the GLIOTRAIN biobank inclusion criteria (Supplementary Table S1, available at <https://doi.org/10.1016/j.annonc.2022.11.008>). FF tumour samples from three participating institutions were collected (Supplementary Table S2, available at <https://doi.org/10.1016/j.annonc.2022.11.008>) and clinical data associated with GLIOTRAIN samples are described in Supplementary Table S3, available at <https://doi.org/10.1016/j.annonc.2022.11.008>.

Validation and Glioma Longitudinal AnalySiS consortium longitudinal cohorts. Transcriptomic and clinical data from The Cancer Genome Atlas Glioblastoma Multiforme (TCGA-GBM) data collection were downloaded from the National Cancer Institute Genomic Data Commons (GDC) data portal (TCGA RNA-seq cohort).¹⁵ mRNAseq_693 (batch 1) dataset and clinical data were downloaded from the Chinese Glioma Genome Atlas database (<http://www.cgga.org.cn>) (CGGA RNA-seq cohort).¹⁶ The DUKE cohort comprised GBM patients treated at Duke's Preston Robert Tisch Brain Tumor Center (RNA sequencing carried out by Caris Life Sciences, Phoenix, AZ). The Glioma Longitudinal AnalySiS (GLASS) dataset (GLASS cohort) was downloaded from Synapse (<https://www.synapse.org/#!Synapse:syn17038081/wiki/585622>).¹⁷ Clinical annotation for DUKE and GLASS datasets was provided by collaborators upon request and are described in Supplementary Tables S3 and S4, available at <https://doi.org/10.1016/j.annonc.2022.11.008>, respectively.

Immunotherapy trial cohorts. Transcriptomic data for GSE121810 were provided upon request (Cloughesy cohort¹³). Transcriptomic data were downloaded from SRAPRJNA482620 (Zhao cohort¹⁸). RNA-seq bam files for the PVSRIPO clinical trial were downloaded from the Genotypes and Phenotypes (dbGaP) database (PVSRIPO cohort). Clinical annotation for all datasets was also provided¹⁹ (Supplementary Tables S5 and S6, available at <https://doi.org/10.1016/j.annonc.2022.11.008>). Discovery, validation, GLASS longitudinal and immunotherapy clinical trial cohorts were filtered as outlined (Supplementary

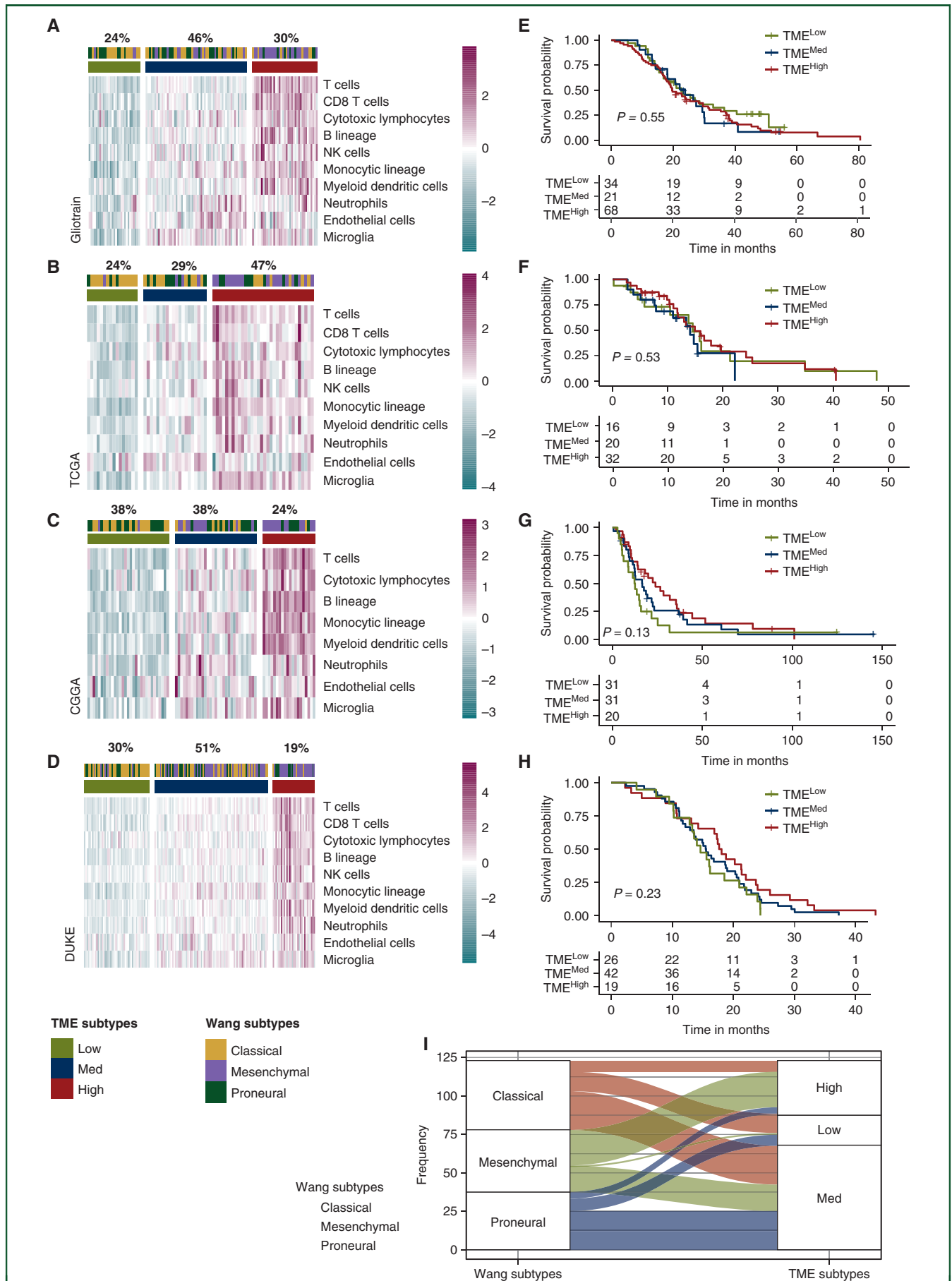


Figure S1, available at <https://doi.org/10.1016/j.annonc.2022.11.008>).

For detailed descriptions of next generation sequencing methods, MCP-counter modification, interrogation of TME composition and validation of novel TME subtypes, Wang subtype classification, neoantigen prediction, multiplexed immunohistochemistry (IHC) methods, IvyGAP dataset analysis, gene ontology (GO) analysis and statistical methods, see [Supplementary Materials](https://doi.org/10.1016/j.annonc.2022.11.008), available at <https://doi.org/10.1016/j.annonc.2022.11.008>.

RESULTS

Modification and validation of MCP-counter for application in GBM

We first established the MCP-counter method for application in GBM (GBM-MCP-counter). Specifically, we removed fibroblast scores, and a GBM-specific microglial signature described by Klemm et al.²⁰ was incorporated. Next, we validated GBM-specific gene expression at the protein level by IHC and immunofluorescence ([Supplementary Figure S2A](https://doi.org/10.1016/j.annonc.2022.11.008), available at <https://doi.org/10.1016/j.annonc.2022.11.008>). Correlations between GBM-MCP scores of immune cell populations and corresponding IHC cell density ([Supplementary Figure S2B](https://doi.org/10.1016/j.annonc.2022.11.008), available at <https://doi.org/10.1016/j.annonc.2022.11.008>) were confirmed. CD3 T cells, CD8 T cells and monocytic lineage showed high correlation coefficients with IHC protein cell density evaluations ($R = 0.43$, $R = 0.52$ and $R = 0.44$, $P = 0.031$, $P = 0.012$ and $P = 0.048$, respectively). Microglia expression signature significantly correlated with microglia immunofluorescence panel cell density (CD68–/Iba1+/TMEM119) ($R = 0.56$, $P = 0.0047$) ([Supplementary Figure S2B](https://doi.org/10.1016/j.annonc.2022.11.008), available at <https://doi.org/10.1016/j.annonc.2022.11.008>).

Identification of novel TME subtypes

PAM clustering, based on patient GBM-MCP-counter scores, was carried out on the GLIOTRAIN cohort. Clustering identified three distinct, novel subtypes with significantly different TME compositions (silhouette statistic methods and principal component analysis) ([Supplementary Figure S3A–D](https://doi.org/10.1016/j.annonc.2022.11.008), available at <https://doi.org/10.1016/j.annonc.2022.11.008>). These subgroups were defined as TME^{Low}, ‘immune-low’, (24%), TME^{Med}, ‘heterogeneous immune populations’, (46%) and TME^{High}, ‘immune-high’, (30%) ([Figure 1A](https://doi.org/10.1016/j.annonc.2022.11.008)). These findings were reproduced in TCGA, CGGA and DUKE datasets ([Figure 1B–D](https://doi.org/10.1016/j.annonc.2022.11.008), [Supplementary Figures S4 and S5](https://doi.org/10.1016/j.annonc.2022.11.008), available at <https://doi.org/10.1016/j.annonc.2022.11.008>). A representative cohort ($N = 26$) from GLIOTRAIN (GLIOTRAIN-IHC cohort) was assigned to TME subtypes

([Supplementary Figure S6A](https://doi.org/10.1016/j.annonc.2022.11.008), available at <https://doi.org/10.1016/j.annonc.2022.11.008>) and quantitative IHC data orthogonally validated each TME subtype ([Supplementary Figure S6B and C](https://doi.org/10.1016/j.annonc.2022.11.008), available at <https://doi.org/10.1016/j.annonc.2022.11.008>).¹⁴ Overall, GBM-MCP-counter analysis revealed that TME^{High} cases are characterised by significantly increased expression of genes specific to all immune populations ([Figure 1A–D](https://doi.org/10.1016/j.annonc.2022.11.008)). TME^{Med} cases were characterised by high endothelial cell GBM-MCP signature and heterogeneous abundance of immune cells. Notably, the microglial signature was enriched in both TME^{High} and TME^{Med} subtypes ([Figure 1A](https://doi.org/10.1016/j.annonc.2022.11.008)). Finally, the TME^{Low} subtype was characterised by a low expression of all immune and endothelial cell markers ([Figure 1A–D](https://doi.org/10.1016/j.annonc.2022.11.008)). Stratification into TME^{High}, TME^{Med} or TME^{Low} subtypes showed no association with overall survival (OS) in GLIOTRAIN, TCGA, CGGA and DUKE cohorts ($P = 0.55$, $P = 0.53$, $P = 0.13$ and $P = 0.55$, respectively) ([Figure 1E–H](https://doi.org/10.1016/j.annonc.2022.11.008)).

We subsequently studied the association of proneural (PN), classical (CL) and mesenchymal (Mes) gene expression subtypes²¹ with novel TME subtypes identified. TME^{High} tumours comprised 23% PN, 18% CL and 59% Mes cases. TME^{Med} comprised 41% PN, 26% CL and 33% Mes cases, and TME^{Low} 55% CL, 35% PN and 10% Mes cases ([Figure 1I](https://doi.org/10.1016/j.annonc.2022.11.008)). The findings remained consistent across all validation cohorts ([Figure 1B–D](https://doi.org/10.1016/j.annonc.2022.11.008)). Survival analysis following Wang subtype patient stratification²¹ (PN, CL, Mes) showed no significant impact on OS in any cohort ([Supplementary Figure S7A–C](https://doi.org/10.1016/j.annonc.2022.11.008), available at <https://doi.org/10.1016/j.annonc.2022.11.008>).

Biological characterisation of TME subtypes

Next, we studied TME composition and functionality across subtypes. Expression of genes associated with functional orientation markers was significantly enriched in the TME^{High} subtype ([Figure 2A](https://doi.org/10.1016/j.annonc.2022.11.008)) in the GLIOTRAIN cohort. Angiogenesis signature expression was homogenous across all TME subtypes ($P = 0.38$) ([Figure 2A](https://doi.org/10.1016/j.annonc.2022.11.008)). The expression of immune-checkpoint-related genes showed a similar trend to immune infiltrate genes, with high expression of genes encoding PD-1 and cytotoxic T-lymphocyte-associated protein 4 (CTLA-4) observed in the TME^{High} subtype ($P = 2.1e-05$, $P = 1.4e-06$) ([Figure 2A](https://doi.org/10.1016/j.annonc.2022.11.008)). CD274 (which encodes PD-L1) was significantly enriched in TME^{High} GBM and heterogeneously expressed across all TME subtypes ($P = 0.0053$), whereas TIM3 was homogeneously expressed across all subtypes ([Figure 2A](https://doi.org/10.1016/j.annonc.2022.11.008), [Supplementary Figure S5A–C](https://doi.org/10.1016/j.annonc.2022.11.008), available at <https://doi.org/10.1016/j.annonc.2022.11.008>). Notably, B7 homolog 3 protein (B7-H3/CD276²²) expression was significantly reduced in TCGA cohort TME^{High} patients

Figure 1. Identification and validation of novel TME subtypes in the GLIOTRAIN cohort and validation datasets (TCGA, CGGA, DUKE).

(A) Partition around medoids (PAM) clustering of the GLIOTRAIN cohort ($N = 123$), based on the cellular TME composition described by MCP-counter scores, reveals three subgroups TME^{Low}, TME^{Med} and TME^{High} in the (B) TCGA, (C) CGGA and (D) DUKE cohorts. OS according to TME^{Low}, TME^{Med} and TME^{High} subtypes in the (E) GLIOTRAIN cohort ($P = 0.55$), (F) TCGA cohort ($P = 0.53$), (G) CGGA cohort ($P = 0.13$) and (H) DUKE cohort ($P = 0.55$). (I) Proportion of Wang subtypes²² in the TME classifiers. Statistical test: (A–D) Kruskal–Wallis one-way analysis of variance; (E–H) P value of log-rank test. CGGA, Chinese Glioma Genome Atlas; CL, classical; Mes, mesenchymal; NK, natural killer; OS, overall survival; PN, proneural; TCGA, The Cancer Genome Atlas; TME, tumour microenvironment.

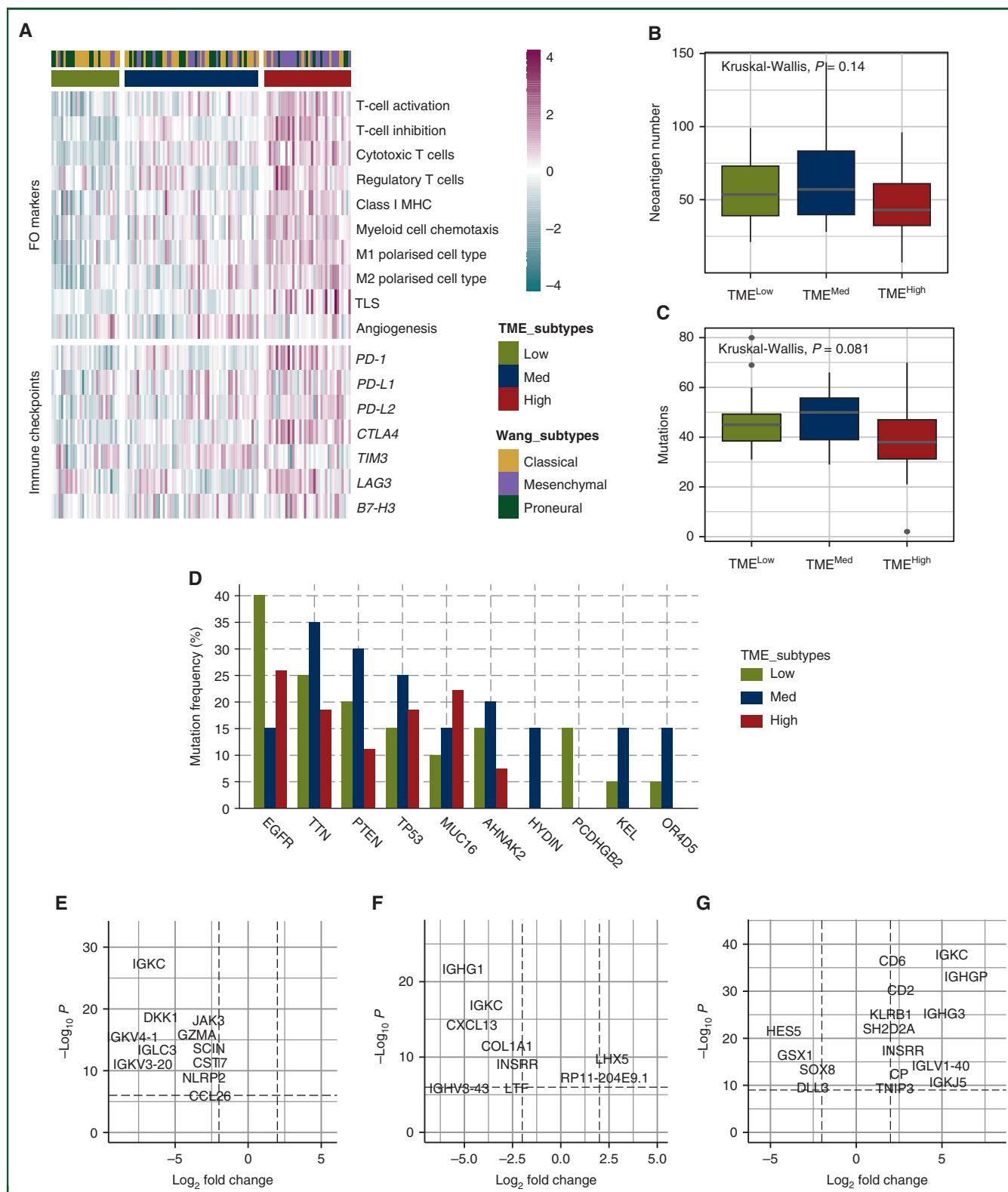


Figure 2. Characterisation of TME subtype-specific biology.

(A) TME functional orientation markers and immune checkpoint expression across TME subtypes in the GLIOTRAIN discovery cohort. (B) Neoeantigen prediction across the TME subtypes in the TCGA cohort. (C) Mutation frequency across the TME subtypes in the TCGA cohort. (D) TME subtype-specific mutation frequency for the top 10 genes with highest frequency in the TCGA cohort. Volcano plots showing differentially expressed genes in (E) TME^{Low}, (F) TME^{Med} and (G) TME^{High} patients. Statistical test: (B, C) Kruskal–Wallis one-way analysis of variance.

CTLA4, cytotoxic T-lymphocyte-associated protein 4; FO, functional orientation; KW, Kruskal–Wallis; MHC, major histocompatibility complex; PD-1, programmed cell death protein 1; PD-L1, programmed death-ligand 1; TCGA, The Cancer Genome Atlas; TLS, tertiary lymphoid structures; TME, tumour microenvironment.

($P = 0.012$; Supplementary Figure S7A, available at <https://doi.org/10.1016/j.annonc.2022.11.008>). No significant difference in B7-H3 expression was observed across novel TME subgroups in other cohorts (Figure 2A, Supplementary Figure S8B and C, available at <https://doi.org/10.1016/j.annonc.2022.11.008>). Interestingly, several previous studies assessing B7-H3 expression in GBM have observed similar diverse expression patterns.²³⁻²⁵

We further interrogated TME subtype mutational landscape within the TCGA RNA-seq cohort, where matching whole exome sequencing data were available. As expected, tumour mutational burden (TMB) was low (median: 48 mutations) (data not shown). Moreover, mutational analysis revealed no difference in neoantigen prediction or mutation count across TME subtypes (Kruskal–Wallis, $P = 0.14$ and $P = 0.081$, respectively) (Figure 2B and C). Nevertheless, a small number of genes were frequently mutated in specific TME subtypes. Specifically, epidermal growth factor receptor (*EGFR*) was most frequently mutated in TME^{Low} GBM, *TTN* in TME^{Med} and *PTEN* in TME^{High} tumours (Figure 2D). Interestingly, IHC analyses (CD20+/CD3+) revealed tertiary lymphoid structures (TLS) as a possible feature of TME^{High}/mesenchymal+ GBM (Supplementary Figure S9A and B, available at <https://doi.org/10.1016/j.annonc.2022.11.008>). Survival analysis in the GLIOTRAIN cohort based on TLS-associated 12-chemokine signature^{26,27} suggested that monocytic lineage in TLS^{High} patients displays suppressed immune responses (Supplementary Figure S9C and D, available at <https://doi.org/10.1016/j.annonc.2022.11.008>). Furthermore, TLS^{High} patients displayed enriched genes associated with T-cell activation and may therefore be able to elicit an immune response (Supplementary Figure S9E, available at <https://doi.org/10.1016/j.annonc.2022.11.008>). We also analysed *MGMT* (O-6-Methylguanine-DNA Methyltransferase) promoter methylation status across novel TME subtypes in the GLIOTRAIN, TCGA, CGGA and DUKE cohorts (Supplementary Figure S10, available at <https://doi.org/10.1016/j.annonc.2022.11.008>). Overall, no significant relationship was observed between *MGMT* status and TME subtype.

Differential gene expression analysis across TME subtypes revealed several genes with significantly reduced expression in the TME^{Low} subtype when compared to non-TME^{Low} samples (Figure 2E). Interestingly, some of the most significantly altered genes (*SLC2A5*, *CSF3R*) were microglial-related. TME^{Med} was associated with several genes with significantly reduced expression, including the B-lymphocyte chemoattractant and TLS marker, *CXCL13* compared to non-TME^{Med} samples (Figure 2F), whereas TME^{High} GBM predominantly consisted genes with significantly increased expression including genes encoding for T lymphocytes (*CD6*), surface antigens on T cells (*CD2*) and cytokine *CCL5* compared to non-TME^{High} samples (Figure 2G). GO enrichment analysis in the GLIOTRAIN cohort revealed TME subtype-specific pathway alterations. TME^{Low} GBM was significantly enriched in pathways relating to EGFR signalling ($P = 0.02406$) (Supplementary Figure S11A, available at <https://doi.org/10.1016/j.annonc.2022.11.008>) and showed

significantly reduced expression of immune-related pathways (Supplementary Figure S12A, available at <https://doi.org/10.1016/j.annonc.2022.11.008>). TME^{Med} was enriched in pathways relating to neuronal signalling (Supplementary Figure S11B, available at <https://doi.org/10.1016/j.annonc.2022.11.008>) and displayed down-regulated immune-related pathways (Supplementary Figure S12B, available at <https://doi.org/10.1016/j.annonc.2022.11.008>). TME^{High} GBM was significantly enriched in pathways relating to the immune system, including complement cascade and immunoregulatory interactions between lymphoid ($P = 2.4e-37$) and non-lymphoid cells ($P = 7.9e-34$) (Supplementary Figure S11C, available at <https://doi.org/10.1016/j.annonc.2022.11.008>). In contrast, few significantly down-regulated pathways were observed in TME^{High} (Supplementary Figure S12C, available at <https://doi.org/10.1016/j.annonc.2022.11.008>).

To address spatial heterogeneity of TME subtype expression signatures, the IvyGAP dataset ($N = 122$ samples) was stratified according to novel TME classifiers (Supplementary Figure S13A, available at <https://doi.org/10.1016/j.annonc.2022.11.008>). Spatial interrogation of TME subtype distribution (based on IvyGAP anatomic neighbourhoods) identified differing gene expression patterns among each anatomic region. TME^{High} samples were most enriched within regions defined as cellular tumour (63%). TME^{High} samples also demonstrated slightly elevated proportions of microvascular proliferation samples (12%) compared to other subtypes. The TME^{Med} cohort manifested a moderate proportion of infiltrating tumour samples (10%) and an elevated proportion of microvascular proliferation samples (15%) compared to TME^{Low} samples (6%). In contrast, TME^{Med} samples displayed the highest proportion of pseudopalisading cells around necrosis samples (23%). Finally, the TME^{Low} cohort contained the highest proportion of infiltrating tumour (14%) and leading edge (12%) samples. An additional subgroup (12.6%), which displayed an enriched expression of endothelial ($P < 2.2e-16$) and myeloid dendritic cells ($P = 3.5e-16$), was further identified upon IvyGAP sample clustering (Cluster EC, Supplementary Figure S13, available at <https://doi.org/10.1016/j.annonc.2022.11.008>). This cluster most frequently manifested with leading edge samples (20%) compared with TME^{Low}, TME^{Med} or TME^{High} subtypes (Supplementary Figure S13B, available at <https://doi.org/10.1016/j.annonc.2022.11.008>).

Longitudinal analysis of TME subtypes reveals TME subtype 'switch' on recurrence

To assess TME subtype evolution and identify changes in TME composition at tumour recurrence, we next analysed a set of longitudinal transcriptomic data from the GLASS longitudinal cohort ($n = 99$ patients with primary and recurrent tumours).¹⁷ Firstly, TME subtypes were applied to primary and recurrent GLASS cohort tumours ($n = 367$ tumour samples representing primary and recurrence 1-4), followed by assessment of functional orientation markers and immune checkpoint expression. These analyses

revealed that T cells, CD8 T cells, B lineage and PD-1 expression were significantly enriched in recurrent tumours (Figure 3A). Next, we categorised the GLASS cohort according to novel TME subtypes (Supplementary Figure S14A, available at <https://doi.org/10.1016/j.annonc.2022.11.008>) identifying a higher proportion of TME^{Med} (39%) and TME^{High} (22%) cases in recurrent samples when compared to primary tumours (33% and 12%, respectively) (Figure 3B and C). The proportion of TME^{Low} tumours decreased from 55% to 39% upon recurrence. Tumours which transitioned from TME^{Low} to TME^{Med} upon recurrence presented significantly elevated lymphocyte-associated gene expression. Specifically, T cells ($P = 5.4e-06$), CD8 T cells ($P = 2.3e-10$), cytotoxic lymphocytes ($P = 0.022$) and B lineage ($P = 0.00085$) expression markers were elevated (Figure 3D). TME^{Low} to TME^{High} transitions revealed significantly enriched lymphocytes and monocytic lineage (Figure 3E). TME^{Med} to TME^{High} subtype transition showed a significant enrichment across immune and stromal cell populations (excluding microglia) (Figure 3F). Unsurprisingly, tumours which switched to more immune cold subtypes displayed significantly decreased immune populations (Supplementary Figure S14B and C, available at <https://doi.org/10.1016/j.annonc.2022.11.008>). In-depth cell-state analysis revealed that TME^{Med} to TME^{High} transition was influenced by a significantly enriched myeloid cell state ($P = 0.0019$). Moreover, stem-like and diff-like neoplastic states were significantly depressed upon this transition ($P = 0.04$ and $P = 0.00049$, respectively) (Supplementary Figure S15A-C, available at <https://doi.org/10.1016/j.annonc.2022.11.008>). Differential gene expression (DEG) analysis revealed several significantly up-regulated chemokine signalling-related pathways upon TME^{Med} to TME^{High} switch (Supplementary Figure S15D, available at <https://doi.org/10.1016/j.annonc.2022.11.008>). Moreover, tumour-promoting chemokines, CCL18 and ACP5, were highly up-regulated upon subtype switch (Supplementary Figure S15E, available at <https://doi.org/10.1016/j.annonc.2022.11.008>). In a very limited number of available longitudinal GLASS cohort samples ($n = 4$) from patients treated with immunotherapy, we assessed whether trends in TME subtype switch are altered following treatment (Supplementary Figure S14D, available at <https://doi.org/10.1016/j.annonc.2022.11.008>). Unsurprisingly, the findings were inconclusive, with transitions from TME^{Med} to TME^{Low} ($n = 1$), TME^{Med} to TME^{High} ($n = 1$) and TME^{Low} to TME^{Med} ($n = 2$) observed.

TME subtypes may inform treatment outcome in retrospective immunotherapy trial datasets

We subsequently examined whether patient stratification based on TME subtype could predict response to immune checkpoint blockade. To this end, we accessed RNA-seq and clinical annotation data from the recent neoadjuvant anti-PD-1 multi-institution clinical trial (Cloughesy cohort).¹³ This trial evaluated immune responses and survival following neoadjuvant and/or adjuvant therapy with

pembrolizumab in patients with recurrent, surgically resectable GBM. Firstly, IDHmt samples ($N = 4$) were identified and excluded. Subsequently, TME classifiers were assigned to the trial cohort (Figure 4A). TME^{High} tumour-bearing patients displayed a trend towards improved OS when compared with TME^{Low} and TME^{Med} tumour-bearing patients ($P = 0.29$) (Figure 4B). Importantly, TME^{High} patients treated with neoadjuvant anti-PD-1 exhibited a significantly increased OS compared with neoadjuvant anti-PD-1-treated non-TME^{High} (TME^{Low} and TME^{Med}) patients and TME^{Med} patients treated with adjuvant anti-PD-1 ($P = 0.028$) (Figure 4C and D).

Next, to further study the relationship between TME subtype and response to ICI, we accessed RNA-seq data from the Zhao et al.'s study (Zhao cohort) which evaluated immune responses and survival of longitudinally profiled patients during standard therapy and following treatment with PD-1 inhibitors (nivolumab or pembrolizumab).¹⁸ Firstly, the GBM-MCP-counter was applied to pre- and post-anti-PD-1-treated tumour samples ($n = 24$) (Figure 5A). Comparison of pre- and post-treatment samples revealed that tumours receiving adjuvant anti-PD-1 displayed no significantly different GBM-MCP scores. Next, samples were assigned to novel TME subtypes. Survival analysis showed a trend towards improved OS in TME^{High} compared to non-TME^{High} patients (TME^{Low}/TME^{Med}) ($P = 0.21$) (Figure 5B). We subsequently assessed how TME subtype proportion changes in pre- and post-anti-PD-1 treatment samples, and in responders and non-responders (responders defined as those which revealed an inflammatory response, few tumour cells upon sampling and stable or shrinking tumour volume). Following anti-PD-1 treatment, the proportion of TME^{Low} tumours remained the same (33%), the proportion of TME^{Med} tumours decreased from 27% to 22% and the proportion of TME^{High} tumours increased from 40% to 44% (Figure 5C). Based on pre-treatment tumour samples, TME^{Low} proportion was greater in responders (7%) compared to non-responders (20%). Likewise, 43% of TME^{High} were responders compared with 40% of non-responders. No TME^{Med} samples were categorised as responders (Supplementary Figure S16, available at <https://doi.org/10.1016/j.annonc.2022.11.008>). Comparison of GBM-MCP scores in non-responders and responders and in pre- and post-ICI-treated ($n = 3$) samples (Supplementary Figure S17, available at <https://doi.org/10.1016/j.annonc.2022.11.008>) indicated no significant changes in TME populations.

Finally, we examined whether patient stratification based on TME subtype could predict response to oncolytic virus therapy. Sequencing and clinical data were accessed from the Desjardins et al.¹⁹ 2018 phase I clinical trial (NCT01491893) which evaluated convection-enhanced intratumoural delivery of recombinant non-pathogenic polio-rhinovirus chimera (PVSRIPO) in rGBM patients (PVSRIPO cohort). Samples were first assigned to TME subtypes (Figure 5E). Tentatively, TME^{High} patients treated with PVSRIPO showed a trend towards improved OS ($P = 0.056$) when compared with TME^{Low} and TME^{Med} tumours (Figure 5E).

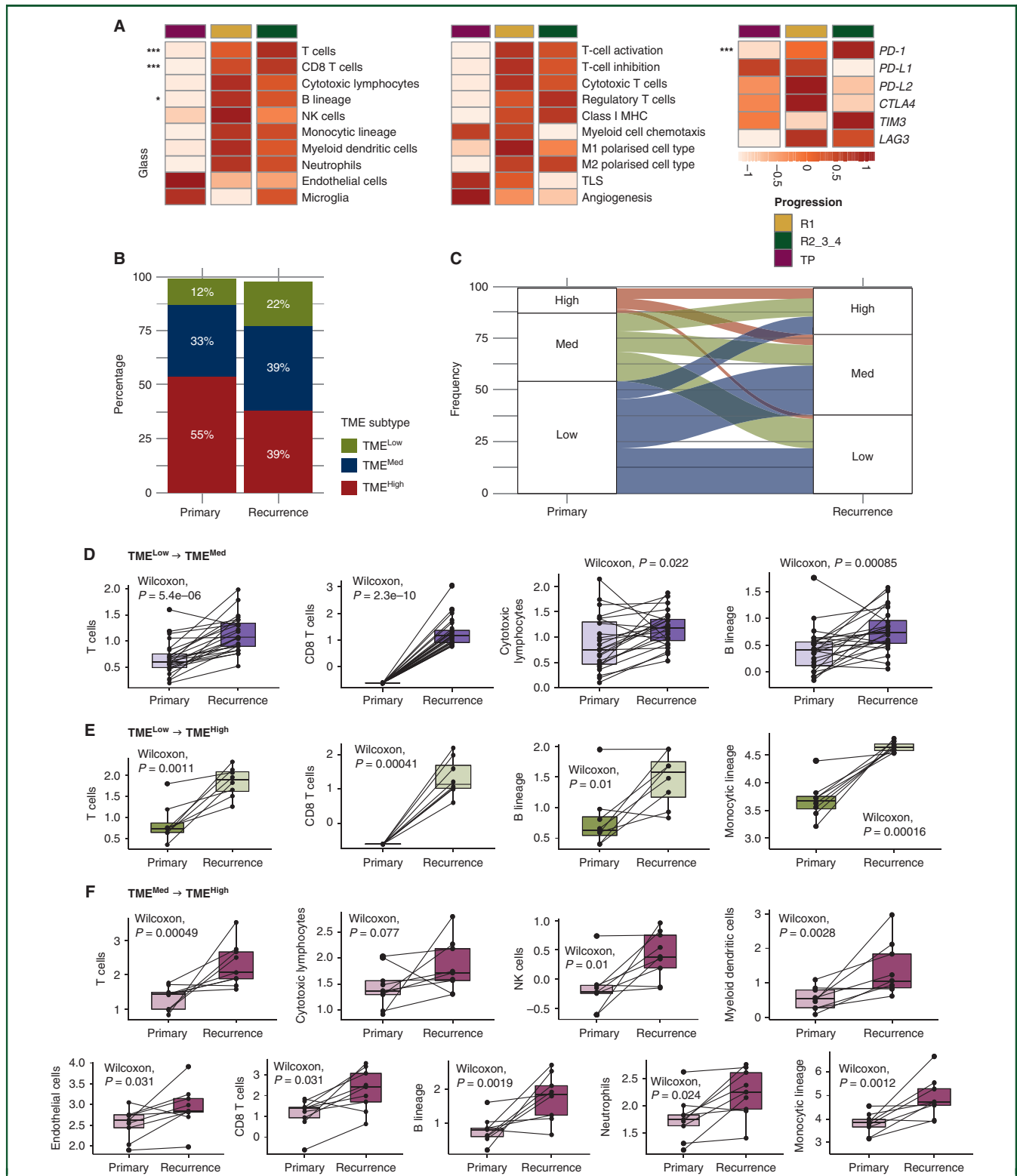


Figure 3. GBM TME and associated TME subtypes exhibit cellular heterogeneity upon recurrence.

(A) Heatmap showing the expression of GBM-MCP scores, FO markers and immune checkpoints in primary tumours (TP), first recurrence (R1) and combined second, third and fourth recurrence in the GLASS cohort. (B) Continuous bar graph showing the distribution of TME subtypes in matching primary and recurrent tumours ($N = 99$ tumour pairs). (C) Sankey plot indicating the transition of TME subtypes on recurrence. Band size reflects sample numbers and band colours represent TME subtype. (D-F) Boxplots showing the TME cell populations with significantly enriched MCP scores from primary to recurrent samples in patients who switch subtype: (D) TME^{Low} (primary) to TME^{Med} (recurrent) tumours, (E) TME^{Low} (primary) to TME^{High} (recurrent) tumours and (F) TME^{Med} (primary) to TME^{High} (recurrent) tumours. Statistical test: Wilcoxon signed rank test. * $P < 0.05$; *** $P < 0.001$. CTLA4, cytotoxic T-lymphocyte-associated protein 4; FO, functional orientation; GBM, glioblastoma; GLASS, Glioma Longitudinal Analysis; MCP, microenvironment cell population; MHC, major histocompatibility complex; NK, natural killer; PD-1, programmed cell death protein 1; PD-L1, programmed death-ligand 1; TLS, tertiary lymphoid structures; TME, tumour microenvironment.

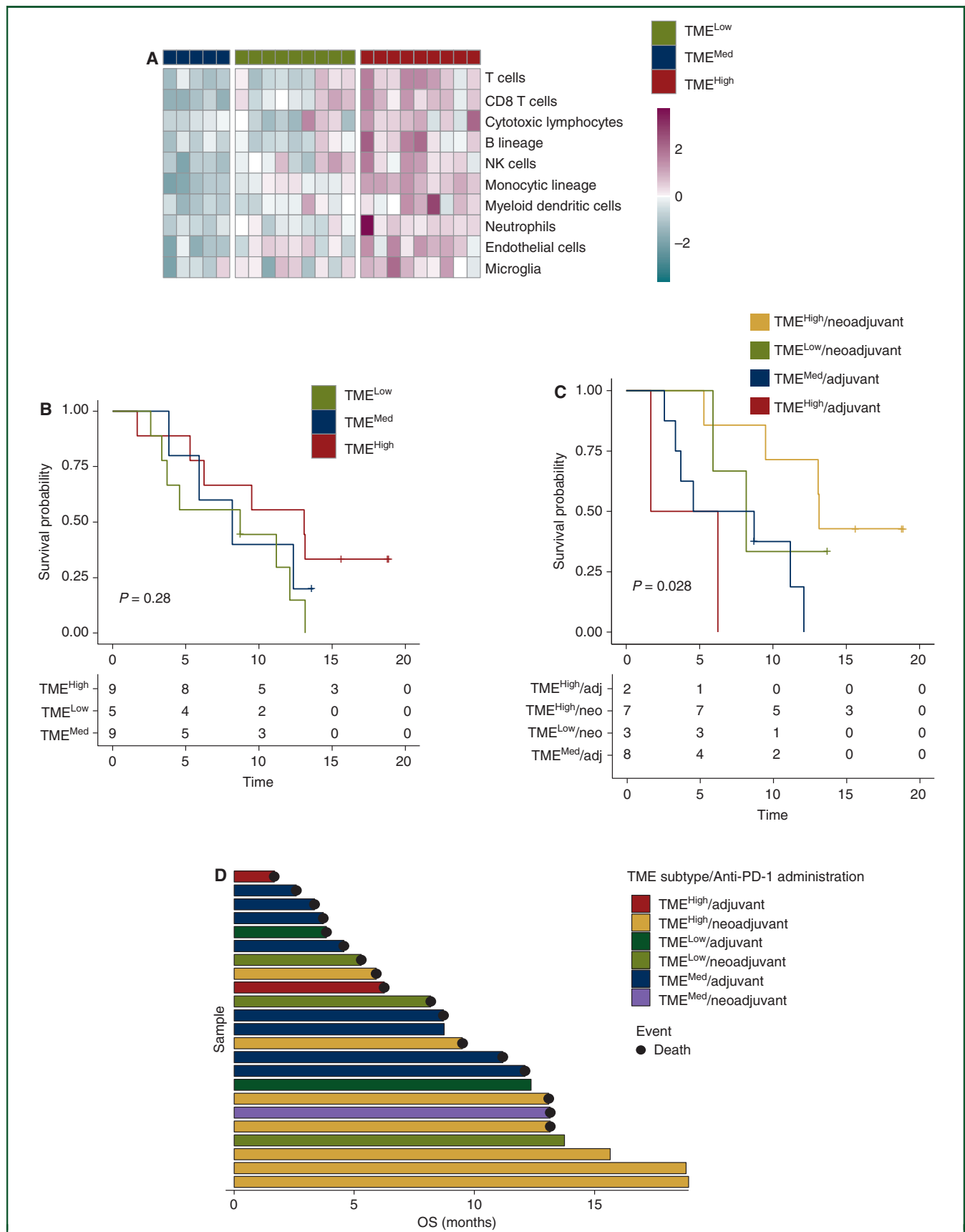


Figure 4. Trend towards improved OS following neoadjuvant pembrolizumab in recurrent IDHwt GBM TME^{High} patients.

DISCUSSION

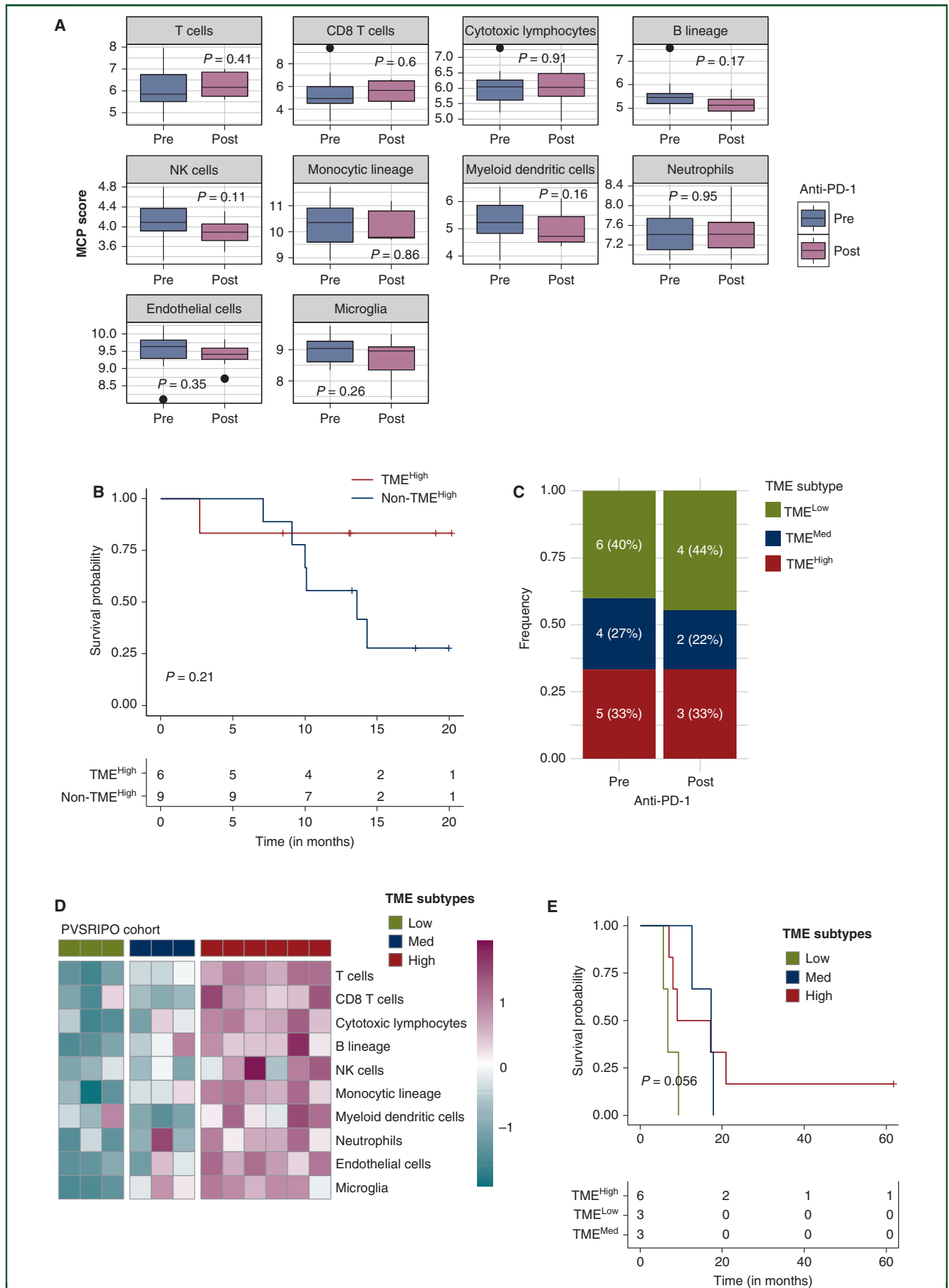
Notwithstanding the plausible rationale which has supported ICI evaluation in GBM trials,^{6,7} to date, clinical studies have largely been negative^{9,10} with few exceptions.^{13,28,29} Of these,^{30,31} recent data from a small multicentre trial (Cloughesy et al.'s study) suggest that neoadjuvant nivolumab may improve OS compared to patients receiving adjuvant therapy.¹³ Furthermore, mechanistic interrogation of the immune microenvironment following administration of neoadjuvant nivolumab revealed increased immune cell infiltration, chemokine transcript expression and greater T-cell antigen receptor diversity among tumour-infiltrating lymphocytes.²⁸ Notwithstanding these important hypothesis-generating data, most negative clinical trial outcomes⁹⁻¹² now mandate the identification of new stratification methods to identify a subpopulation of patients for whom immunotherapy could be a viable option. To this end, we hypothesised that interrogation of the TME, including the identification of novel TME-associated subtypes, might predict which patients would be most responsive to immunotherapy and have generated robust hypotheses for novel subtype-specific combinatorial immunotherapy treatment regimens, which now warrant further testing.²

To identify novel TME-specific classifiers, we implemented a tailored, brain tumour-specific MCP-counter¹⁴ method. Specifically, unsupervised PAM clustering was applied to GBM-MCP-counter scores in discovery and validation cohorts ($N = 867$ primary/recurrent patient samples) to identify three non-overlapping TME subtypes: TME^{Low}, TME^{Med} and TME^{High}. Survival analysis revealed that there was no subtype-specific prognostic association. This is unsurprising as discovery and validation cohorts were normalised for Karnofsky Performance score (KPS) and age and included only IDHwt samples. Moreover, GBM-MCP-counter scores are based on genes which have no clear prognostic value when assessed as individual biomarkers.³⁰ We observed an overlap between novel TME subtypes and Wang transcriptomic classifiers. However, we observed no survival differences following classification according to Wang subtypes.²¹ There was no significant difference in neoantigen load across TME classifiers, and a low TMB was observed across all subtypes. Interestingly, Zhang et al. recently showed that methylated MGMT and low *TIM3* expression are associated with improved survival in GBM.³¹ However, in our analyses, *TIM3* expression was homogeneous across subtypes. No significant relationship was observed between MGMT methylation status and novel TME subtype.

TME^{Low} GBM is associated with low immune and endothelial cell abundance, low expression of genes associated with TME functional orientation and overall down-regulated immune-regulatory pathways. TME^{Low} tumours also manifested the highest proportion of infiltrating tumour and leading edge samples within the IvyGAP cohort compared to TME^{High} and TME^{Med} patient samples. Mutational and GO analysis showed that EGFR mutation and up-regulated EGFR signalling pathways were dominant features of TME^{Low} GBM. As TME^{Low} patients exhibit overall low immune cell abundance, our data indicate that patients categorised as TME^{Low} may be the most suitable candidates for a prospective clinical trial evaluating the combination of anti-TIM3 with an EGFR inhibitor. This strategy would concurrently target the high EGFR mutational burden of TME^{Low} patients whilst stimulating T-cell infiltration. Recently, it has been suggested that EGFR therapeutic resistance may arise due to extrachromosomal DNA (ecDNA) amplification, rather than classical chromosomal alterations.³² Further interrogation of TME^{Low} ecDNA landscape is required to uncover potential resistance mechanisms which may be hallmarks of this subtype.

TME^{Med} GBM is associated with an abundance of immune populations, functional orientation markers, immune checkpoint and endothelial cell markers. TME subtype analysis of IvyGAP anatomical samples revealed that TME^{Med} patients comprised the highest proportion of samples defined as 'pseudopalisading cells around necrosis'. Interestingly, pseudopalisades are associated with microvascular hyperplasia and angiogenesis, and may serve as predictors of poor prognosis in GBM.³³ Thus, despite negative outcomes following anti-angiogenic therapy (NCT00884741 and CheckMate-143/NCT02017717), our data tentatively suggest that patients identified in the 'colder' TME^{Med} subtype may benefit from anti-angiogenic treatment combined with immunotherapy due to high endothelial cell abundance, vascularity and diverse immune cell population. Additionally, titin (TTN) mutation was identified as a TME^{Med} tumour feature. While TTN mutations are associated with favourable prognosis in non-small-cell lung cancer,³⁴ mutant TTN may be associated with an increased risk of glioma recurrence³⁵ suggesting that TTN mutations could influence GBM TME^{Med} tumour recurrence. GO analysis of TME^{Med} tumours further revealed up-regulated neuronal system-related and transmission across chemical synapses pathways. We and others have recently shown that increased GBM growth and invasion is facilitated by neuron-to-glioma synapses and increased neuronal interactions at recurrence.^{36,37} Overall,

(A) Partition around medoids (PAM) clustering of IDHwt GBM samples in the Cloughesy cohort¹³ with available RNA-seq data ($N = 23$), based on the cellular TME composition described by GBM-MCP-counter scores, reveals three subtypes: TME^{Low}, TME^{Med} and TME^{High}. (B) OS according to TME^{Low}, TME^{Med} and TME^{High} subtypes in the Cloughesy cohort. (C) OS according to TME^{Low}/neoadjuvant anti-PD-1, TME^{Med}/adjuvant anti-PD-1, TME^{High}/adjuvant anti-PD-1 and TME^{High}/adjuvant patients in the Cloughesy cohort. TME^{Med} patients treated with neoadjuvant anti-PD-1 ($N = 1$) and TME^{Low} patients treated with adjuvant anti-PD-1 ($N = 2$) were excluded due to small patient numbers. (D) Swimmer plot representing OS of patients in the Cloughesy cohort. Bars are colour coded according to the patients' TME subtype and whether they received neoadjuvant + adjuvant (neo) anti-PD-1 therapy or adjuvant (adj) anti-PD-1 alone. Statistical test: Kaplan-Meier analysis; P value of log-rank test. GBM, glioblastoma; IDHwt, isocitrate dehydrogenase wild type; NK, natural killer; OS, overall survival; PD-1, programmed cell death protein 1; TME, tumour microenvironment.



future studies are now required to interrogate the role of TTN and neuronal-tumour interactions in TME^{Med} GBM recurrence and tumour progression.

TME^{High} tumours were defined by high immune cell infiltration and abundance of endothelial cells. Additionally, TME^{High} tumours are enriched for markers associated with T-cell activation, major histocompatibility complex I genes, myeloid cell chemotaxis, inhibitory T cells, regulatory T cells, tumour-associated macrophage and immune checkpoints. These markers are indicative of a highly immunosuppressive, tumour-promoting environment.^{38,39} Targeting specific cell populations to alleviate immunosuppression in TME^{High} GBM will likely be required to maximise response to immunotherapy. Interestingly, 65% of TME^{High} tumours were identified as Mes, suggesting that a subpopulation of Mes patients may respond to ICI, with TME subtyping representing a more refined predictive classification approach. TME subtype analysis of IvyGAP anatomical samples revealed that TME^{High} patients comprised the highest proportion of samples defined as ‘microvascular proliferation’ regions, a classic hallmark of GBM. DEG and GO analysis in TME^{High} tumours further revealed several up-regulated genes and pathways related to immunoregulation. Interestingly, TLSs (and an associated transcriptomic signature) were specifically identified in TME^{High}/mesenchymal+ tumours. TLSs have been associated with clinical benefit and response to immunotherapy in solid tumours;⁴⁰ however, the clinical relevance of TLSs in GBM remains unclear.⁴¹ Our data suggest that monocytic lineage abundance may influence mechanisms which impact OS of TLS^{High} patients. The immunosuppressive role of TAMs^{27,42} and their role in inducing a mesenchymal-like state in GBM⁴³ are well documented. Thus, in TME^{High} GBM, TAMs may suppress TLS antitumour activity, hindering immunotherapy response. Future studies to confirm the promiscuity of TLSs and associated subsets of immunosuppressive macrophages in TME^{High} tumours are warranted.⁴⁴ Overall, our data suggest that targeting anti-PD-1 + anti-CTLA4 may be a viable approach although it is noteworthy that a previous phase I trial identified concerning treatment-related adverse effects (AEs) in rGBM patients treated with combinatorial nivolumab and ipilimumab therapy, followed by nivolumab monotherapy. Specifically, grade 3/4 AEs were reported in 90% of patients who received 1 mg/kg nivolumab plus 3 mg/kg ipilimumab (NIVO1 + IPI3), and 30% of patients who received 3 mg/kg nivolumab plus 1 mg/kg ipilimumab (NIVO3 + IPI1).¹¹ A rational alternative strategy in this sub-cohort could be anti-PD-1 + TAM targeting (e.g. colony-stimulating factor-1 receptor inhibitor).

Longitudinal assessment of TME subtypes has also revealed their dynamic nature. Tumours which transitioned from TME^{Low} to TME^{Med} or TME^{High}, and TME^{Med} to TME^{High}, were associated with significantly enriched lymphocytes, myeloid population abundance, T-cell functionality and an immunosuppressive TME. Importantly, we and others have recently shown that IDHwt GBM recurrence may be attributed to increased immune cell composition and presence of a myeloid cell state. Moreover, this enriched myeloid cell state is associated with a mesenchymal subtype shift.³⁶ Here, we investigated whether TME subtypes are driven from a ‘lower to higher’ TME status by changes in the neoplastic (proliferative stem-like, stem-like and differentiated-like) and myeloid cell state upon recurrence.³⁶ Our data suggest that TME^{Med} to TME^{High} switch is influenced by a distinct myeloid phenotype, decreased tumour cell differentiation and up-regulated chemokine signalling pathways. Moreover, CCL18 (promotes glioma progression) and ACP5 (mediator of glioma growth) were highly up-regulated upon subtype switching.^{45,46} Overall, this pathway may harbour potential therapeutic avenues for the treatment of patients with tumours which transition from TME^{Med} to TME^{High} upon recurrence. To further understand subtype evolution and treatment resistance, single-cell RNA-seq analysis and construction of dynamic cellular models to inform TME plasticity, cellular lineage and trajectory is now required. It will also be important to consider whether therapeutic pressure may truly drive subtype switching.^{40,47} Additional analyses of biopsies in primary and recurrent tumours (post-treatment) may further unravel the impact of intratumoural heterogeneity on TME subtype classification and TME subtype-specific treatment resistance mechanisms.³⁶

Finally, the predictive potential of novel TME subtypes was retrospectively assessed in interventional immunotherapy clinical trial datasets. Firstly, our analysis of the small Cloughesy trial dataset tentatively suggests that TME^{High} patients who receive neoadjuvant anti-PD-1 might show improved OS compared to patients receiving adjuvant anti-PD-1 alone. Nevertheless, we acknowledge that TME stratification before neoadjuvant treatment is not without complexity. However, we hypothesise that in the future, TME subtyping might be carried out before surgery by using a blood-based cell-free RNA liquid biopsy method,⁴⁸ or a robust TME subtype-specific magnetic resonance imaging radiomic signature.^{49,50} Secondly, analysis of the Zhao cohort suggests that TME^{High} tumour-bearing patients trend towards improved OS following anti-PD-1 therapy. In a very limited subset of matched samples collected pre- and

Figure 5. Trend towards improved OS and increased response rate in TME^{High} patients following adjuvant treatment with pembrolizumab or PVSRIPO.

(A) TME composition in Zhao dataset¹⁸ pre- versus post-adjuvant anti-PD-1 treatment in available tumour ($N = 24$) samples. (B) OS according to TME^{High} and non-TME^{High} (TME^{Low} + TME^{Med}) subtypes who received adjuvant anti-PD-1 therapy in the Zhao cohort ($N = 15$ patients). (C) Relative boxplots indicating the proportion of TME^{Low}, TME^{Med} and TME^{High} patients before administration of anti-PD-1 treatment (left) and after anti-PD-1 treatment (right) in available tumour and blood samples. (D) Partition around medoids (PAM) clustering of the PVSRIPO cohort¹⁹ with available RNA-seq data ($N = 12$), based on the cellular TME composition described by GBM-MCP-counter scores, reveals three subtypes: TME^{Low}, TME^{Med} and TME^{High}. (E) OS according to TME^{Low} and TME^{Med} and TME^{High} subtypes who received PVSRIPO therapy in the PVSRIPO cohort.¹⁹ Statistical test: Wilcoxon signed rank test. Kaplan–Meier analysis; P value of log-rank test. GBM, glioblastoma; MCP, microenvironment cell population; NK, natural killer; OS, overall survival; PD-1, programmed cell death protein 1; TME, tumour microenvironment.

post-ICI therapy ($n = 3$ patients), no significant alterations were detected in MCP scores before or after treatment (Supplementary Figure S17, available at <https://doi.org/10.1016/j.annonc.2022.11.008>). As mentioned previously, conclusions with respect to subtype switching may not be drawn from such a limited number of samples. Thus, further studies in expanded patient cohorts are now warranted. Interestingly, a relationship between TME subtype assigned at the time of primary tumour resection and response to anti-PD-1 was observed regardless of the standard-of-care treatment regimen before anti-PD-1 therapy. This observation also requires further validation. Thirdly, we investigated whether TME subtypes were predictive of survival within the small PSVRIP0 dataset (NCT01491893). Here, GBM patients received adjuvant anti-PD-1 (newly diagnosed) or PVSRIPO therapy (recurrent tumours, treatment administered post-biopsy). Stratification of PVSRIPO patients based on TME subtypes suggests a trend towards improved OS in TME^{High} patients, compared with TME^{Med} and TME^{Low} patients. Clearly, these hypothesis-generating data now require validation in larger clinical cohorts. Desjardins et al. recently showed that a low mutational burden was associated with increased tumour-intrinsic inflammation in rGBM and increased response to PVSRIPO treatment.⁵¹ Interestingly, our data suggest that TME^{High} patients may harbour a lower mutational burden than other subtypes, yet represent the subtype with the highest proportion of ICI responders.

Overall, as mentioned, while we observe promising trends in all trial cohorts assessed, sample numbers are limited. Moreover, each trial cohort analysed has a unique study design and implements a specific immunotherapy regimen. Furthermore, an important study limitation is that validation of our findings in an expanded cohort of samples from recently conducted negative phase III trials (e.g. CheckMate-143, CheckMate-548 and CheckMate-498) has not been possible due to lack of availability of tissue/RNA-seq data. A tailored phase II study using a rational hypothesis-driven trial design is now required to validate our findings. This trial should mandate for the robust collection of FF tissue for retrospective molecular analysis.

In conclusion, our multicentre study introduces novel TME subtypes which may inform optimal precision immunotherapy treatment strategies in the GBM setting. Our data provide convincing evidence that a TME subtype classification system represents a canonical ‘*terminus a quo*’ (starting point) to (i) deepen knowledge of GBM TME biology, (ii) support identification of patient subgroups who may benefit from immunotherapy and/or other TME targeting agents and (iii) provide a platform for the identification of new TME-associated contexts of vulnerability. Our findings warrant further investigation in additional retrospective immunotherapy trial cohorts and in the prospective setting.

ACKNOWLEDGEMENTS

The work presented in this paper is dedicated to the memory of Mr Paolo Iacovelli. We would like to thank J.

Heffernan, L. M. Houlihan and J. Mythen (Beaumont Hospital Neuropathology Department) for their help in establishing the GLIOTRAIN biobank in Dublin. The authors gratefully acknowledge all patients who kindly donated tumour tissue and clinical/genomic data used in this study.

FUNDING

This project has received funding from the European Union’s Horizon 2020 and 2021 research and innovation programme under the Marie Skłodowska-Curie ITN initiatives [grant number #766069], GLIOTRAIN (<http://www.gliotrain.eu>) and ‘GLIORESOLVE’ projects [grant number #101073386]. Additional support was received by donation from the Paolo Iacovelli memorial endowment. We are also grateful for the financial support from the Beaumont Hospital Foundation, and from Brain Tumour Ireland to establish the Beaumont Hospital Brain Tumour Biorepository. The authors further acknowledge financial contribution towards staff salaries from RCSI and Champions Oncology (Baltimore, USA).

DISCLOSURE

The authors have declared no conflicts of interest.

REFERENCES

1. Brat DJ, Aldape K, Colman H, et al. cIMPACT-NOW update 5: recommended grading criteria and terminologies for IDH-mutant astrocytomas. *Acta Neuropathol.* 2020;139(3):603-608.
2. White K, Connor K, Clerkin J, et al. New hints towards a precision medicine strategy for IDH wild-type glioblastoma. *Ann Oncol.* 2020;31:1679-1692.
3. Schiffer D, Annovazzi L, Casalone C, Corona C, Mellai M. Glioblastoma: microenvironment and niche concept. *Cancers (Basel).* 2018;11:5.
4. Berghoff AS, Kiesel B, Widhalm G, et al. Programmed death ligand 1 expression and tumor-infiltrating lymphocytes in glioblastoma. *Neuro Oncol.* 2015;17(8):1064-1075.
5. Nduom EK, Wei J, Yaghi NK, et al. PD-L1 expression and prognostic impact in glioblastoma. *Neuro Oncol.* 2016;18(2):195-205.
6. Preusser M, Lim M, Hafner DA, Reardon DA, Sampson JH. Prospects of immune checkpoint modulators in the treatment of glioblastoma. *Nat Rev Neurol.* 2015;11(9):504-514.
7. Reardon DA, Gokhale PC, Klein SR, et al. Glioblastoma eradication following immune checkpoint blockade in an orthotopic, immunocompetent model. *Cancer Immunol Res.* 2016;4(2):124-135.
8. Yuan B, Wang G, Tang X, Tong A, Zhou L. Immunotherapy of glioblastoma: recent advances and future prospects. *Hum Vaccin Immunother.* 2022;18(5):1-16.
9. Reardon DA, Brandes AA, Omuro A, et al. Effect of nivolumab vs bevacizumab in patients with recurrent glioblastoma: the CheckMate 143 phase 3 randomized clinical trial. *JAMA Oncol.* 2020;6(7):1003-1010.
10. Bristol Myers Squibb. Bristol Myers Squibb: Checkmate-548; 2019. Available at <https://tinyurl.com/j6v2zkkj>. Accessed April 21, 2022.
11. Omuro A, Vlahovic G, Lim M, et al. Nivolumab with or without ipilimumab in patients with recurrent glioblastoma: results from exploratory phase I cohorts of CheckMate 143. *Neuro Oncol.* 2018;20(5):674-686.
12. Bristol-Myers Squibb. Bristol-Myers Squibb Announces Phase 3 CheckMate-498 Study Did Not Meet Primary Endpoint of Overall Survival with Opdivo (nivolumab) Plus Radiation in Patients with Newly Diagnosed MGMT-Unmethylated Glioblastoma Multiforme; 2019. Available at <https://news.bms.com/news/corporate-financial/2019/Bristol-Myers-Squibb-Announces-Phase-3-CheckMate-498-Study-Did-Not-Meet-Primary-Endpoint-of-Overall-Survival-with-Opdivo-nivolumab-Plus>

- Radiation-in-Patients-with-Newly-Diagnosed-MGMT-Unmethylated-Glio-blastoma-Multiforme/default.aspx. Accessed May 4, 2022.
13. Cloughesy TF, Mochizuki AY, Orpilla JR, et al. Neoadjuvant anti-PD-1 immunotherapy promotes a survival benefit with intratumoral and systemic immune responses in recurrent glioblastoma. *Nat Med*. 2019;25(3):477-486.
 14. Becht E, Giraldo NA, Lacroix L, et al. Estimating the population abundance of tissue-infiltrating immune and stromal cell populations using gene expression. *Genome Biol*. 2016;17(1):218.
 15. McLendon R, Friedman A, Bigner D, et al. Comprehensive genomic characterization defines human glioblastoma genes and core pathways. *Nature*. 2008;455(7216):1061-1068.
 16. Zhao Z, Zhang KN, Wang Q, et al. Chinese Glioma Genome Atlas (CGGA): a comprehensive resource with functional genomic data from Chinese glioma patients. *Genomics Proteomics Bioinformatics*. 2021;19(1):1-12.
 17. Aldape K, Amin SB, Ashley DM, et al. Glioma through the looking GLASS: molecular evolution of diffuse gliomas and the Glioma Longitudinal Analysis Consortium. *Neuro Oncol*. 2018;20(7):873-884.
 18. Zhao J, Chen AX, Gartrell RD, et al. Immune and genomic correlates of response to anti-PD-1 immunotherapy in glioblastoma. *Nat Med*. 2019;25(3):462-469.
 19. Desjardins A, Gromeier M, Herndon JE 2nd, et al. Recurrent glioblastoma treated with recombinant poliovirus. *N Engl J Med*. 2018;379(2):150-161.
 20. Klemm F, Maas RR, Bowman RL, et al. Interrogation of the microenvironmental landscape in brain tumors reveals disease-specific alterations of immune cells. *Cell*. 2020;181(7):1643-1660.e17.
 21. Wang Q, Hu B, Hu X, et al. Tumor evolution of glioma-intrinsic gene expression subtypes associates with immunological changes in the microenvironment. *Cancer Cell*. 2017;32(1):42-56.e6.
 22. Nehama D, di Ianni N, Musio S, et al. B7-H3-redirected chimeric antigen receptor T cells target glioblastoma and neurospheres. *EBioMedicine*. 2019;47:33-43.
 23. Zhang J, Wang J, Marzese DM, et al. B7H3 regulates differentiation and serves as a potential biomarker and theranostic target for human glioblastoma. *Lab Invest*. 2019;99(8):1117-1129.
 24. Zhang C, Zhang Z, Li F, et al. Large-scale analysis reveals the specific clinical and immune features of B7-H3 in glioma. *Oncoimmunology*. 2018;7(11):e1461304.
 25. Digregorio M, Coppieters N, Lombard A, Lumapat PN, Scholtes F, Rogister B. The expression of B7-H3 isoforms in newly diagnosed glioblastoma and recurrence and their functional role. *Acta Neuropathol Commun*. 2021;9(1):59.
 26. Coppola D, Nebozhyn M, Khalil F, et al. Unique ectopic lymph node-like structures present in human primary colorectal carcinoma are identified by immune gene array profiling. *Am J Pathol*. 2011;179(1):37-45.
 27. Sautès-Fridman C, Petitprez F, Calderaro J, Fridman WH. Tertiary lymphoid structures in the era of cancer immunotherapy. *Nat Rev Cancer*. 2019;19:307-325.
 28. Schalper KA, Rodriguez-Ruiz ME, Diez-Valle R, et al. Neoadjuvant nivolumab modifies the tumor immune microenvironment in resectable glioblastoma. *Nat Med*. 2019;25(3):470-476.
 29. Lee AH, Sun L, Mochizuki AY, et al. Neoadjuvant PD-1 blockade induces T cell and cDC1 activation but fails to overcome the immunosuppressive tumor associated macrophages in recurrent glioblastoma. *Nat Commun*. 2021;12(1):6938.
 30. Kan LK, Drummond K, Hunn M, Williams D, O'Brien TJ, Monif M. Potential biomarkers and challenges in glioma diagnosis, therapy and prognosis. *BMJ Neurol Open*. 2020;2(2):e000069.
 31. Zhang J, Sai K, Wang XL, et al. Tim-3 expression and MGMT methylation status association with survival in glioblastoma. *Front Pharmacol*. 2020;11:584652.
 32. Nathanson DA, Gini B, Mottahedeh J, et al. Targeted therapy resistance mediated by dynamic regulation of extrachromosomal mutant EGFR DNA. *Science*. 2014;343(6166):72-76.
 33. Brat DJ, van Meir EG. Vaso-occlusive and prothrombotic mechanisms associated with tumor hypoxia, necrosis, and accelerated growth in glioblastoma. *Lab Invest*. 2004;84:397-405.
 34. Cheng X, Yin H, Fu J, et al. Aggregate analysis based on TCGA: TTN missense mutation correlates with favorable prognosis in lung squamous cell carcinoma. *J Cancer Res Clin Oncol*. 2019;145(4):1027-1035.
 35. Wu P, Yang W, Ma J, et al. Mutant-allele tumor heterogeneity in malignant glioma effectively predicts neoplastic recurrence. *Oncol Lett*. 2019;18(6):6108-6116.
 36. Varn FS, Johnson KC, Martinek J, et al. Glioma progression is shaped by genetic evolution and microenvironment interactions. *Cell*. 2022;185(12):2184-2199.e16.
 37. Johnson KC, Anderson KJ, Courtois ET, et al. Single-cell multimodal glioma analyses identify epigenetic regulators of cellular plasticity and environmental stress response. *Nat Genet*. 2021;53(10):1456-1468.
 38. Togashi Y, Shitara K, Nishikawa H. Regulatory T cells in cancer immunosuppression - implications for anticancer therapy. *Nat Rev Clin Oncol*. 2019;16:356-371.
 39. Takenaka MC, Gabriely G, Rothhammer V, et al. Control of tumor-associated macrophages and T cells in glioblastoma via AHR and CD39. *Nat Neurosci*. 2019;22(5):729-740.
 40. Neftel C, Laffy J, Filbin MG, et al. An integrative model of cellular states, plasticity, and genetics for glioblastoma. *Cell*. 2019;178(4):835-849.e21.
 41. van de Walle T, Vaccaro A, Ramachandran M, Pietilä I, Essand M, Dimberg A. Tertiary lymphoid structures in the central nervous system: implications for glioblastoma. *Front Immunol*. 2021;12:724739.
 42. Petitprez F, Lévy S, Sun CM, et al. The murine microenvironment cell population counter method to estimate abundance of tissue-infiltrating immune and stromal cell populations in murine samples using gene expression. *bioRxiv*. 2021;39(6):779-792.e11.
 43. Hara T, Chanoch-Myers R, Mathewson ND, et al. Interactions between cancer cells and immune cells drive transitions to mesenchymal-like states in glioblastoma. *Cancer Cell*. 2021;39(6):779-792.e11.
 44. Goswami S, Walle T, Cornish AE, et al. Immune profiling of human tumors identifies CD73 as a combinatorial target in glioblastoma. *Nat Med*. 2020;26:39-46.
 45. Huang Y, Motta E, Nanvuma C, et al. Microglia/macrophage-derived human CCL18 promotes glioma progression via CCR8-ACP5 axis analyzed in humanized slice model. *Cell Rep*. 2022;39(2):110670.
 46. Grochans S, Korbecki J, Simińska D, et al. CCL18 expression is higher in a glioblastoma multiforme tumor than in the peritumoral area and causes the migration of tumor cells sensitized by hypoxia. *Int J Mol Sci*. 2022;23(15):8536.
 47. Chaligne R, Gaiti F, Silverbush D, et al. Epigenetic encoding, heritability and plasticity of glioma transcriptional cell states. *Nat Genet*. 2021;53(10):1469-1479.
 48. Müller Bark J, Kulasinghe A, Chua B, Day BW, Punyadeera C. Circulating biomarkers in patients with glioblastoma. *Br J Cancer*. 2020;122:295-305.
 49. Zhang Z, He K, Wang Z, et al. Multiparametric MRI radiomics for the early prediction of response to chemoradiotherapy in patients with postoperative residual gliomas: an initial study. *Front Oncol*. 2021;11:779202.
 50. Park JE, Kim HS, Jo Y, et al. Radiomics prognostication model in glioblastoma using diffusion- and perfusion-weighted MRI. *Sci Rep*. 2020;10(1):4250.
 51. Gromeier M, Brown MC, Zhang G, et al. Very low mutation burden is a feature of inflamed recurrent glioblastomas responsive to cancer immunotherapy. *Nat Commun*. 2021;12(1):1-7.

APPENDIX 1***GLIOTRAIN consortium***

Annette Byrne <annettebyrne@rcsi.ie>
Kieron White <kieronwhite@rcsi.ie>
Kate Connor <kateconnor@rcsi.ie>
Alice O'Farrell <aliceofarrell@rcsi.ie>
Catherine Fridman <catherine.fridman@crc.jussieu.fr>
Hervé Fridman <herve.fridman@crc.jussieu.fr>
Manuela Salvucci <manuelasalvucci@rcsi.ie>
Jochen Prehn <JPrehn@rcsi.ie>
Archita Biswas <architabiswas@rcsi.ie>
Diether Lambrechts <diether.lambrechts@kuleuven.be>
Ingrid Arijs <ingrid.arijs@kuleuven.vib.be>

Gonca Dilcan Durdag <gonca.dilcandurdag@kuleuven.be>
Francesca Lodi <francesca.lodi@kuleuven.be>
Gabriele Bergers <gabriele.bergers@kuleuven.be>
Jenny Weng <linqian.weng@kuleuven.be>
Maite Verreault <maite.verreault@icm-institute.org>
Ahmed Id Baih <ahmed.idbaih@aphp.fr>
Franck Bielle <franck.bielle@aphp.fr>
Martine Lamfers <m.lamfers@erasmusmc.nl>
Sieger Leenstra <s.leenstra@erasmusmc.nl>
Ioannis Ntafoulis <i.ntafoulis@erasmusmc.nl>
Federica Fabro <f.fabro@erasmusmc.nl>
Andreas Kremer <andreas.kremer@ittm-solutions.com>
Romain Tching <romain.tching@ittm-solutions.com>